PHYSICAL REVIEW B **80**, 060202(R) (2009)

Phase transition in $Ti_{50}Ni_{44}Fe_6$ studied by x-ray fluorescence holography

Wen Hu,[1,2] Kouichi Hayashi,[1,*] Tokujiro Yamamoto,[1] Naohisa Happo,[3] Shinya Hosokawa,[4] Tomoyuki Terai,[5] Takashi Fukuda,[5] Tomoyuki Kakeshita,[5] Honglan Xie,[2] Tiqiao Xiao,[2] and Motohiro Suzuki[6]

[1]*Institute of Materials Research, Tohoku University, Sendai 980-8577, Japan*

[2]*Shanghai Institute of Applied Physics, Chinese Academy of Sciences, Shanghai 201-800, People's Republic of China*

[3]*Graduate School of Information Sciences, Hiroshima City University, Hiroshima 731-3194, Japan*

[4]*Center for Materials Research Using Third-Generation Synchrotron Radiation Facilities, Hiroshima Institute of Technology, Hiroshima 731-5193, Japan*

[5]*Division of Materials and Manufacturing Science, Graduate School of Engineering, Osaka University, Suita 565-0871, Japan*

[6]*SPring-8/JASRI, Hyogo 679-5198, Japan*

(Received 11 June 2009; published 28 August 2009)

The phase transition behavior of the local structure around Fe in a shape-memory-alloy-related material, $Ti_{50}Ni_{44}Fe_6$, was evaluated by x-ray fluorescence holography. The Fe $K\alpha$ holograms were recorded at 225 and 100 K, which correspond to the parent and commensurate phases, respectively. The atomic images at both the phases show that the first neighbor Ti atoms around Fe, fluctuating in the parent phase, is strongly stabilized in the commensurate phase and that a clusterlike structure with a radius of 8 Å is formed in this lower temperature phase. These dynamically structural changes offer important keys to understanding the precursors to the martensite phase transition of the TiNi series.

DOI: 10.1103/PhysRevB.80.060202 PACS number(s): 64.70.Rh, 42.40.−i, 64.70.kd

Shape memory alloys (SMAs) are promising materials for actuators because they exhibit large reversible strain and strong recovery forces upon repeated heating and cooling. These features of SMAs are due to a reversible phase transition, i.e., the martensitic transition, between the parent and martensite phases. In order to achieve larger strain and stronger forces, the martensitic transition has been widely studied for various SMAs. The martensitic transition is a first-order phase transition since the transition is accompanied by a discrete change in volume or other properties. Leading to first-order transformations, it has been experimentally reported for many materials that gradual changes in the lattice modulation,[1] phonon dispersion,[2] and elastic modulus are observed before the martensitic transition starts upon cooling. These gradual changes are attracting much interest as precursors of the martensitic transition, similarly to tweed microstructure that appears upon cooling prior to many other phase transitions, e.g., Guinier-Preston (GP) zone formation, spinodal decomposition, and ordering.[3–8] These phenomena have been also studied by molecular-dynamics simulation and *ab initio* calculation.[9–11] However, studies of the precursors are difficult because they are immediately followed by the main martensitic transition.

Ti-Ni alloys, which are the most practical SMAs, exhibit two kinds of martensitic transitions. One is a direct first-order phase transition from the $B2$ parent phase (P phase) to the $B19'$ martensite phase, and the other is a sequence of first-order phase transitions from the $B2$ phase to the R phase and from the R phase to the $B19'$ phase. Recently, it was found that these first-order phase transitions in $Ti_{50}Ni_{50-x}Fe_x$ are suppressed with increasing Fe content, and only the precursor phenomena are observed when more than 6 at. % of Fe atoms are substituted for Ni.[12] This precursor phenomena of $Ti_{50}Ni_{50-x}Fe_x$ are recognized as a second-order-like transition from the P phase to the incommensurate phase (IC phase). Particularly for $Ti_{50}Ni_{44}Fe_6$, a commensurate phase (C phase) appears upon further cooling. The R and C phases have a similarity that superlattice diffraction spots, such as $\frac{1}{3}\frac{1}{3}0$ diffraction, are observed in selected-area electron-diffraction patterns. Therefore, $Ti_{50}Ni_{44}Fe_6$ is a suitable sample for investigating the lattice modulation accompanied by the appearance of the superlattice structure.

X-ray fluorescence holography (XFH) is a technique for the determination of local structures around a selected fluorescing atom in a solid with no prior model.[13–15] It can yield scattering information without the phase ambiguity inherent in ordinary diffraction methods. The inverse XFH mode[14] applied here uses fluorescing atoms as inner detector to record the interference between the direct incident and scattered x-rays. The three-dimensional (3D) atomic arrangement around a specified element can be observed in direct space by a Fourier transformationlike reconstruction method, which helps to define more precisely the atomic environments over the 15th coordination shells.[15] Recently, we conducted the XFH experiment of $Ti_{50}Ni_{44}Fe_6$ and compared the atomic images at the P and C phases.[16] Subsequently, further analysis was carried out and it revealed the fine changes of the atomic arrangement induced by a phase transition, which will provide hints to the lattice modulation related to the precursor of the martensite phase transitions of SMAs. In this Rapid Communication, we will show different local environments at the P and C phases and discuss the atomic dynamics related to the phase transition.

$Ti_{50}Ni_{44}Fe_6$ exhibits a P-IC transition at 220 K and an IC-C transition at 180 K.[12] In this Rapid Communication, the temperatures of 225 and 100 K were chosen for obtaining holograms in the P and C phases, respectively. The single-crystal $Ti_{50}Ni_{44}Fe_6$ alloy was grown by a floating-zone method. The sample was about 6 mm in diameter with a surface orientation of (110). The lattice constant is $a=3.01$ Å, which was determined by x-ray diffraction. The XFH experiment was carried out at beamline BL6C of the Photon Factory at KEK, Tsukuba, Japan. The x-ray beam

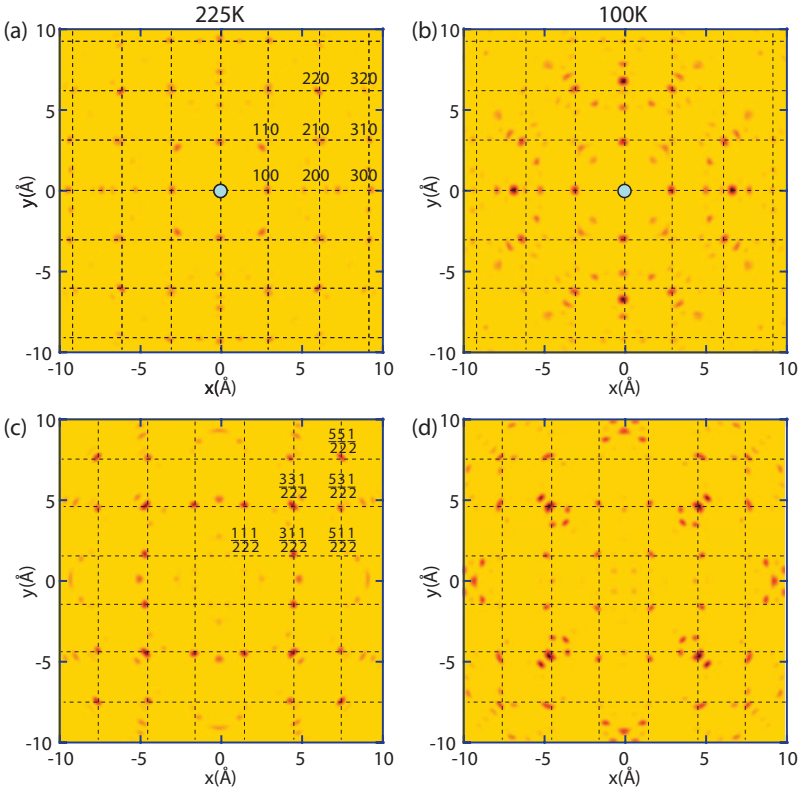

FIG. 1. (Color) Atomic images on the (001) lattice plane at $z=0$ Å (upper) and $z=1.5$ Å (lower) in the P (left) and C phases (right). The intersections of the dotted lines indicate the ideal positions of the Ni/Fe atoms in (a) and (b) and the Ti atoms in (c) and (d).

from the bending magnet source was monochromatized by a Si (111) double-crystal monochromator and focused onto the sample with a Si bent total reflection mirror. The incident x-ray energies were 8.0–12.0 keV in 0.5 keV steps. Using the toroidally bent graphite crystal, Fe $K\alpha$ fluorescent x rays from the sample were analyzed and focused onto an avalanche photodiode. The fluorescence intensities were recorded by scanning the azimuthal angle of the sample ϕ in the range of $0° \leq \phi \leq 360°$ and the incident angle θ in the range of $0° \leq \theta \leq 70°$, each in 1° steps. Details of the setup are given elsewhere.[15] The measurement time for one single-energy hologram was about 7 h. The intensity of each pixel was about 3×10^5 counts. The sample was cooled to 225 K from room temperature at rate of 1.6 K/min and then was cooled again to 100 K after 3 days of XFH measurement. The x-ray absorption fine structure (XAFS) was also measured near the Fe K absorption edge at 100 and 225 K at beamline BL01B2 of SPring-8.

The intensities of fluorescent x rays were normalized to the incident x-ray intensities and the hologram oscillation data were obtained by subtracting the background. The hologram data were extended to the 4π sphere using the $Pm3m$ crystal symmetry of the present sample[17] and the x-ray standing-wave lines observed in the raw data.

Figures 1(a) and 1(b) show the images on the typical Ni/Fe atomic plane at $z=0$ Å in the P (225 K) and C (100 K) phases, respectively. The intersections of the dotted lines indicate the ideal atomic positions of Ni/Fe atoms. Although the intensities of the atomic images decrease with increasing distance from the emitter Fe in both the phases, their tendencies are different. Namely, the image intensities of the neighboring atoms of the C phase given in Fig. 1(b), such as those at 100, 200, and 210 positions, are higher than those in Fig. 1(a). In contrast, the far atomic images in Fig. 1(b), such as those located at 300, 310, and 320 positions, in the C phase are weaker than those in the P phase in Fig. 1(a).

Figures 1(c) and 1(d) exhibit the atomic images of the Ti planes ($z=1.5$ Å) in the P and C phases, respectively. From the comparison of these two figures, only the images of the first neighbor Ti atoms have a large difference; these images are very weak for the P phase but markedly clear for the C phase. The intensity ratio of the first neighbor Ti in the C and P phases is 2.2, but such a large intensity change is not observed in other Ti atomic images. The radial distribution functions around Fe were obtained from the XAFS data. However, such a large difference of the first neighbor Ti peak intensity was not observed between the C and P phases.

To ascertain what occurs at the atomic level during the phase transition, we focus on the two anomalies mentioned above, i.e., (1) the image intensities of the first neighbor Ti atoms are drastically enhanced at low temperature and (2) the images of the distant Ni/Fe atoms in the C phase are weaker than those in the P phase. The intensity of all atomic images gradually increases with decreasing temperature owing to the suppression of the thermal agitation effect indicated by the Debye-Waller factor.[15] However, the above two findings cannot be explained by a simple Debye-Waller effect.

In order to understand the observation of the first neighbor Ti atomic images, we introduce an atomic model with a positional fluctuation. Since the spatial resolution of XFH images is about 0.5 Å,[18] atomic distributions within 0.5 Å are not resolved by this method. However, such a spatial atomic fluctuation largely affects the XFH image intensity.

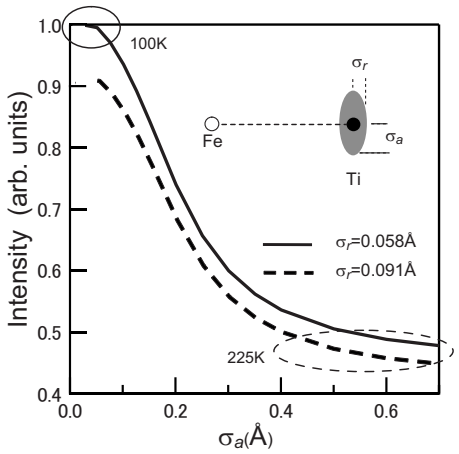

FIG. 2. Distribution dependence of the intensity of the first neighbor. The solid and dashed curves correspond to the image intensity at 100 and 225 K, respectively. Fe and Ti spots indicate a model of the central emitter and one of its first neighbor atoms. σ_a and σ_r correspond to the displacement of first neighbor Ti atoms along the radial and angular directions, respectively.

We performed a theoretical calculation of image intensities. The average length of the Fe-Ti bonds was fixed to be 2.61 Å, which was obtained from the XAFS, and does not change greatly with temperature. The XAFS data also provided the mean-square displacement along the radial direction, σ_r, which is estimated to be 0.091 Å at 225 K and 0.058 Å at 100 K. We fixed the σ_r values and calculated the intensities of the atomic images by changing the mean-square displacement along the angular direction, σ_a.

Figure 2 shows the σ_a dependence of the intensity of the first neighbor Ti images at 100 (solid curve) and 225 K (dashed curve). Both the theoretical intensities rapidly decrease with increasing σ_a in the small σ_a region below 0.2 Å and then saturate in the large σ_a region beyond 0.4 Å. From this calculation, it is suggested that the large intensity difference between the first neighbor Ti atoms of the *C* (100K) and *P* (225 K) phases with the ratio of 2.2 can be realized only when σ_a in the *C* phase is a very small value lower than 0.1 Å, similar to the σ_r value, and that in the *P* phase is larger than 0.4 Å.

Next, we discuss the behavior of the Ni/Fe atomic image intensities at the distant atoms in the *C* phase. In order to clarify the intensity changes upon the phase transition, each intensity ratio of the atomic images in the *C* and *P* phases was calculated. Figures 3(a) and 3(b) show the intensity ratios given on the Ni/Fe atomic plane at $z=0$ Å and at $z=3.0$ Å, respectively. The ratios are converted to the lightness of the spots. The images of neighboring Ni/Fe atoms within the radius of about 8 Å indicated by dashed circle are enhanced in the *C* phase. To confirm the intensity change as a function of the distance from the center when a normal *B*2 structure is assumed, we calculated theoretical holograms using a cluster model with 28 326 atoms for nine incident energies and obtained the intensity of each atomic image from their reconstructions. The tendency of the intensity change depending on the distance in the *P* phase is similar to that obtained from the present calculation, and the atomic image

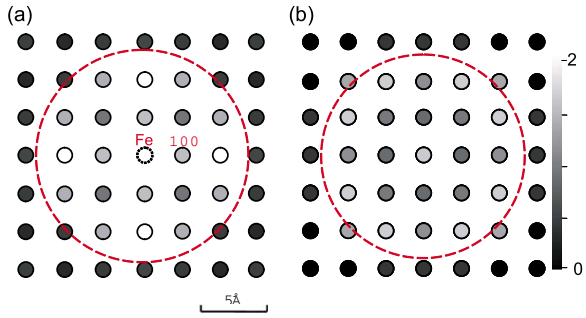

FIG. 3. (Color online) Atomic arrangements of Ni/Fe planes with intensity ratios of *C* and *P* phases at (a) $z=0$ Å and (b) $z=3.0$ Å. The dashed circles with the radius of 8 Å indicate the area of a clusterlike structure in the *C* phase at 100 K. The gray bar indicates the intensity ratios of the *C* and *P* phases. The lightness shows the atomic image enhancement due to phase transition to *C* phase.

in the *P* phase can be explained by the presence of a uniform *B*2 structure of $Ti_{50}Ni_{44}Fe_6$. Contrary to this, the distance dependence of the intensity at the *C* phase is largely different from the calculated one. Thus, to interpret the atomic images at the *C* phase, a more complex structure model is necessary.

As already discussed, the large spatial fluctuation of the atoms results in diminishing the intensity of the atomic image. As seen in Fig. 3, the atomic positions within about 8 Å around the Fe atom are strongly fixed in the *C* phase, and the atoms outside this range are disordered. This finding indicates the existence of a clusterlike structure in which the atoms are frozen. However, an Fe atom need not be only at the center of the cluster as in Fig. 3 because the cluster includes about four Fe atoms as estimated from the concentration. Even with Fe atoms at any position in the 8 Å sphere, such a clusterlike image will be displayed in the reconstruction because the 3D images obtained by XFH are averaged local structures. A structure with domain size of a few nm was reported in a TEM dark-field image of the *C* phase,[12] which would be related with the formation of the clusterlike structure found by the present XFH measurement.

For the intensity ratios of Ti atomic images at 100 and 225 K, on the contrary, such a clusterlike structure cannot be seen because of a large errors in their intensities. The atomic images of the light Ti atoms may be strongly affected by the holographic oscillations from the heavy Ni or Fe atoms.

We have separately discussed two topics concerning the stabilization of the first neighbor Ti atom and the formation of the clusterlike structure. However, it is very likely that these two phenomena are closely related to each other. The dopant Fe atoms cause the positions of the first Ti atoms to fluctuate in the *P* phase. This distortion plays an important role in maintaining the uniform atomic arrangement of $Ti_{50}Ni_{44}Fe_6$. On the other hand, because of the suppression of the fluctuation in the *C* phase, the atoms in the clusterlike structures are self-organized in their positions and become locally stable. Since such clusters are not suitable for forming a entire crystal, the atoms between the clusters may disorder to bridge the clusters, and thus the image intensities of the distant atoms are diminished. Moreover, the formation of

the clusterlike structure may reflect the appearance of the superlattice structure observed by electron diffraction.[12]

Martensitic transitions do not accompany atomic diffusion. Structural change from the *P* phase to the martensite phase is achieved by collective atomic movement, such as shear or shuffling of the lattice planes. Taking into account the fact that $Ti_{50}Ni_{44}Fe_6$ shows the *P*-IC-*C* transition instead of the martensitic transition, a certain number of the clusterlike structures may disturb the collective atomic movement because of the barrier of their boundaries. However, the superlattice structure, which causes a similar electron-diffraction pattern to the *R* phase, is still observed in the IC or *C* phase in $Ti_{50}Ni_{44}Fe_6$ (Ref. 12) even though the *R* phase transformation was suppressed. It should be noted here that the morphology of the domain with the superlattice structure observed in the IC or *C* phase is similar to that of the ω phase formed in β-Ti and Zr alloys martensitically rather than that of the *R* phase of TiNi alloys.[19]

It was proposed that displacement of lattice plane accompanies the β to ω transition.[5,6,20–23] Point defects such as substitutions of atoms seem to play an important role in the β to ω transition, and the displacement of lattice planes induces locally lattice softening for the phase transition, as proposed by Clapp.[21] As reported by Satija *et al.*[24] and Moine *et al.*,[25] the TA_2 transverse acoustical phonon branch along [100] shows a minimum around $\langle\frac{1}{3}\frac{1}{3}0\rangle 2\pi/a$ as a precursor of *R* phase transformation. Moreover, Ohba *et al.*[26] reported that phonon softening also shows a minimum, although *R* phase transformation is not observed in $Ti_{50}Ni_{44}Fe_6$. Therefore, it is implied that the formation of the superlattice domain also induces phonon softening in $Ti_{50}Ni_{44}Fe_6$.

Several clusterlike structures are embedded in the superlattice domain in $Ti_{50}Ni_{44}Fe_6$. It is possible to consider that the martensitic formation of the superlattice domain, such as the *P*-IC phase transition, is induced by a colony of the several clusterlike structures in the *P* phase, which plays a role of a nucleus or an embryo. Therefore, we speculate that since the clusterlike structures start to form in the *P* phase in advance of martensitic *P*-IC phase transition, the atomistic structural revolution of forming the clusterlike structures in the *P* phase induces the lattice softening as a precursor phenomenon.

In summary, we have discussed the dynamics of the phase transition of $Ti_{50}Ni_{44}Fe_6$ on the basis of the 3D images obtained by XFH, i.e., the formation of the cluster with a size of 8 Å in the *C* phase. We believe that our findings provide an important hint to understanding the mechanism of the martensite phase transition of the TiNi series. Note that such structural information cannot be obtained by other methods, and the present results indicate a possible application of the XFH.

W.H., H.L.X., and T.Q.X. would like to thank the China Scholarship Council and National Natural Science Foundation of China (Grant No. 10505028) for financial support. The authors thank S. Sasaki of Tokyo Institute of Technology for support in the XFH experiment. A part of this work was financially supported by a Grant-in-Aid for Scientific Research (B) (Grant No. 18360300) from the Ministry of Education, Culture, Sports, Science and Technology of Japan. The XFH experiments were performed at BL-6C of PF/KEK (Proposal Nos. 2007G514 and 2007G573).

*khayashi@imr.tohoku.ac.jp

[1] P. Moine, G. M. Michal, and R. Sinclair, Acta Metall. **30**, 109 (1982).
[2] A. Heiming, W. Petry, J. Trampenau, M. Alba, C. Herzig, H. R. Schober, and G. Vogl, Phys. Rev. B **43**, 10948 (1991).
[3] T. E. Stenger and J. Trivisonno, Phys. Rev. B **57**, 2735 (1998).
[4] L. E. Tanner, Philos. Mag. **14**, 111 (1966).
[5] C. S. Becquart, P. C. Clapp, and J. A. Rifkin, Phys. Rev. B **48**, 6 (1993).
[6] S. Kartha, T. Castan, J. A. Krumhansl, and J. P. Sethna, Phys. Rev. Lett. **67**, 3630 (1991).
[7] K. B. Rundman and J. E. Hilliard, Acta Metall. **15**, 1025 (1967).
[8] S. Semenovskaya and A. G. Khachaturyan, Phys. Rev. Lett. **67**, 2223 (1991).
[9] R. Meyer and P. Entel, Phys. Rev. B **57**, 5140 (1998).
[10] U. Pinsook and G. J. Ackland, Phys. Rev. B **59**, 13642 (1999).
[11] K. Parlinski and M. Parlinska-Wojtan, Phys. Rev. B **66**, 064307 (2002).
[12] M.-S. Choi, T. Fukuda, T. Kakeshita, and H. Mori, Philos. Mag. **86**, 67 (2006).
[13] M. Tegze and G. Faigel, Nature (London) **380**, 49 (1996).
[14] T. Gog, P. M. Len, G. Materlik, D. Bahr, C. S. Fadley, and C. Sanchez-Hanke, Phys. Rev. Lett. **76**, 3132 (1996).
[15] K. Hayashi, Adv. Imaging Electron Phys. **140**, 119 (2006).
[16] W. Hu, K. Hayashi, N. Happo, S. Hosokawa, T. Terai, T. Fukuda, T. Kakeshita, H. Xie, and T. Xiao, J. Cryst. Growth **311**, 982 (2009).
[17] G. Burns and A. M. Glazer, *Space Group for Solid State Scientists*, 2nd ed. (Academic Press, Boston, 1990).
[18] M. Tegze, G. Faigel, S. Marchesini, M. Belakhovsky, and A. I. Chumakov, Phys. Rev. Lett. **82**, 4847 (1999).
[19] S. L. Sass, J. Less-Common Met. **28**, 157 (1972).
[20] D. De Fontaine and O. Buck, Philos. Mag. **27**, 967 (1973).
[21] P. C. Clapp, Phys. Status Solidi B **57**, 561 (1973) b.
[22] P. Georgopoulos and J. B. Cohen, Acta Metall. **29**, 1535 (1981).
[23] S. M. Shapiro, B. X. Yang, Y. Noda, L. E. Tanner, and D. Schryvers, Phys. Rev. B **44**, 9301 (1991).
[24] S. K. Satija, S. M. Shapiro, M. B. Salamon, and C. M. Wayman, Phys. Rev. B **29**, 6031 (1984).
[25] P. Moine, J. Allain, and B. Renker, J. Phys. F: Met. Phys. **14**, 2517 (1984).
[26] T. Ohba, D. Kitanosono, S. Morito, T. Fukuda, T. Kakeshita, A. Q. R. Baron, and S. Tsutsui, Mater. Sci. Eng., A **481-482**, 254 (2008).